Journal of Scientific Computing (2020) 82:81
https://doi.org/10.1007/s10915-020-01185-1

# A Total Fractional-Order Variation Model for Image Super-Resolution and Its SAV Algorithm

**Wenjuan Yao[1] · Jie Shen[2] · Zhichang Guo[1] · Jiebao Sun[1] · Boying Wu[1]**

Received: 30 September 2019 / Revised: 31 January 2020 / Accepted: 7 March 2020


**Abstract**
Single-image super-resolution reconstruction aims to obtain a high-resolution image from a low-resolution image. Since the super-resolution problem is ill-posed, it is common to use a regularization technique. However, the choice of the fidelity and regularization terms is not obvious, and it plays a major role in the quality of the desired high resolution image. In this paper, a hybrid single-image super-resolution model integrated with total variation (TV) and fractional-order TV is proposed to provide an effective reconstruction of the HR image. We develop an efficient numerical scheme for this model using the scalar auxiliary variable approach with an adaptive time stepping strategy. Thorough experimental results suggest that the proposed model and numerical scheme can reconstruct high quality results both quantitatively and perceptually.

**Keywords** Fractional-order variation · Super resolution · Scalar auxiliary variable · Texture

## 1 Introduction

Single image super-resolution (SR), also known as image scaling up or image enhancement, aims at estimating a high-resolution (HR) image from a low-resolution (LR) observed image. As a fundamental problem in image processing, it has been extensively studied over the

✉ Zhichang Guo
mathgzc@hit.edu.cn

Wenjuan Yao
mathywj@126.com

Jie Shen
shen7@purdue.edu

Jiebao Sun
sunjiebao@hit.edu.cn

Boying Wu
mathwby@hit.edu.cn

[1] School of Mathematics, Harbin Institute of Technology, Harbin, China

[2] Department of Mathematics, Purdue University, West Lafayette, IN 47907, USA

Published online: 14 March 2020

past few decades and has many important applications in areas such as remote sensing [1], hyperspectral [2], medical imaging [3], and consumer electronics [4].

Let $\Omega_L$ be a subset of $\Omega \subset \mathbb{R}^2$. We define a low resolution image $f$ as a real function defined in $\Omega_L$ and assume that high resolution images are defined on the whose domain $\Omega$. We consider a down-sampling linear operator $D$ acting on high resolution images with values in low resolution ones. The relationship between the observed image $f$ and the unknown high resolution image $u$ can be formulated as

$$f = Hu + n, \tag{1}$$

where $Hu = D(h * u)$, $h$ is a given translation invariant convolution kernel and $n$ is Gaussian white noise with zero mean and variance $\sigma^2$. The kernel $h$ is determined as the point spread function (PSF) of the sensor.

A large number of SR approaches have been developed. These techniques can be roughly divided into three categories: interpolation-based methods [5,6], example learning-based methods [7–9] and reconstruction-based methods [10–12].

The interpolation-based methods exploit base functions or interpolation kernels to estimate the unknown pixels in the HR grid. By using linear, bilinear, cubic algorithm, the methods of this family are comparatively simple and with relatively low computational complexity [13–15]. However, these methods are more likely to produce ringing and jagged artifacts when handling large magnification factors or small input images [16]. Consequently, the SR capability of this family of methods may be insufficient in some applications.

The example learning-based methods typically exploit a training database composed of LR and HR image patch pairs to infer the mapping relationship between the LR and HR feature space. Then, the learned mapping relationship is used to recover the missing high-frequency details of an input LR image. Extensive research results have demonstrated their powerful SR capabilities [17–21]. However, the methods of this family usually require a large number of image samples for learning and perform complicated learning process with high computation complexity.

Reconstruction-based methods [22,23] generate a HR image based on designed degradation model. In the regularization framework, where HR image is estimated based on some prior knowledge about the image (e.g., degree of smoothness) in the form of regularization, the SR problem turns out to be well posed [24]. Particularly, Tikhonov regularization [25] based on bounded variation (BV) ($L^2$ norm) is one of the popular regularization methods for SR reconstruction. It imposes smoothness in reconstructed image, but at the same time loses some details (e.g., edges) present in the image. In order to preserve the edge in the image, the regularization method based on total variation (TV) ($L^1$ norm) is developed for image restoration [26]. However, quite a few techniques [27–29] are available to handle non-differentiable TV regularization efficiently. Particularly, Marquina and Osher [30] are first to use Bregman iteration for fast SR image reconstruction with TV regularization.

Many partial differential equation (PDE)-based image restoration techniques utilize TV regularization due to its discontinuity (edge) preserving property. However, this method favors solutions that are piecewise constant, which results in the staircasing effect in recovered images. There have been many efforts to improve the performance of TV by using higher-order regularization. In [31,32], the second-order TV regularization was proposed to reduce the staircasing effects. Though these methods can eliminate the staircase effect efficiently, they often lead to a speckle effect. While those traditional TV based approaches to image restoration result in sharper images, they yield an unnatural cartoon-like image, compromising on the quality of, and almost eliminating, textures. The reason is that TV based methods are based upon local operators while textures are essentially nonlocal in nature [33].

As a nonlocal operator, fractional-order differential has been introduced recently as a regularization term, leading to some fractional differential-based variational models. Up to now, fractional differential-based methods have been frequently used in many image processing fields such as image denoising [34] and SR reconstruction [35]. Particularly, Bai and Feng [36] proposed a new class of fractional order anisotropic diffusion equations for noise removal. For ease of calculation, Pu et al. [37] implemented a class of fractional differential masks and illustrated that fractional differentiation can deal well with fine structures like texture information. Those results illustrated that fractional differential-based approach can better enhance texture details than integral-based algorithms.

Although various types of SR reconstruction methods have been proposed to solve the ill-posed inverse problem in SR, few could perform well in preserving textures in HR images. Accordingly, finding a method that can recover the lost details is a major challenge in reconstruction-based methods, which is also a goal of this paper. In order to obtain an effective image prior, it is of great importance to model the appropriate feature of natural images. The combination of different types of prior knowledge makes a better model for characterizing various image features and benefits the SR performance. Based on the advantages of the TV-based regularization and the fractional differential-based regularization, a hybrid term is proposed in this paper, which increases the quality of the restoration step of the SR process. Particularly, the proposed model would perform well in preserving both edges and texture details of the image.

Another goal of this paper is to develop an efficient numerical scheme for the proposed model. More precisely, we utilize the recently developed Scalar Auxiliary Variable (SAV) approach [38,39] to construct an unconditionally energy diminishing, fast and easy to implement algorithm. Different from usual optimization algorithms, this approach does not introduce many auxiliary parameters that affect the efficiency of the whole algorithm, and its convergence rate can be accelerated with an adaptive time stepping strategy.

In summary, the proposed hybrid variational method enjoys the following features:

- It combines total variation filter with a fractional order filter, which can unite the advantages of the two filters, and has a remarkable effect in improving the quality of the recovered HR images, in terms of preserving edges and texture details of images.
- The existence of the minimizer function of the proposed variational model is analyzed theoretically.
- An efficient energy diminishing numerical scheme based on the SAV approach is developed along with an adaptive time stepping to accelerate the convergence.
- Numerical results indicate that the proposed algorithm recovers well edges and captures small features not appearing in the low resolution images. In contrast to state of art methods, our proposed approach performs better both visually and quantitatively.

The remainder of this paper is organized as follows. In Sect. 2, we review the total $\alpha$-order variation and the space of functions of fractional-order bounded variations. Then we give some properties of this space. Section 3 introduces a hybrid model and SAV algorithm in detail. In Sect. 4, we present extensive experiments and corresponding analysis. The conclusion is summarized in Sect. 5.

## 2 Preliminaries

In this section, we recall a fractional total $\alpha$-order regularizer and detail some properties of the $\alpha$-bounded variation space in [40]. As a generalization of TV regularizers, the fractional

total $\alpha$-order variation is defined as follows:

$$\mathrm{TV}^{\alpha}(u) = \sup_{\mathbf{v}} \left\{ \int_{\Omega} (-u \mathrm{div}^{\alpha} \mathbf{v}) \mathrm{d}x \,|\, \mathbf{v} = (v_1, v_2) \in \left( C_0^l(\Omega, \mathbb{R}^2) \right)^2, \|\mathbf{v}\|_{L^\infty} < 1 \right\}, \quad (2)$$

where $0 \leqslant l = n - 1 < \alpha < n$, $\|\mathbf{v}\|_{L^\infty} = \max \sqrt{v_1^2 + v_2^2}$, $\mathrm{div}^{\alpha} v = \frac{\partial^{\alpha} v_1}{\partial x_1^{\alpha}} + \frac{\partial^{\alpha} v_2}{\partial x_2^{\alpha}}$ and $\frac{\partial^{\alpha} v_i}{\partial x_i^{\alpha}}$ denotes a fractional $\alpha$-order derivative of $v_i$ along the $x_i$ direction. $C_0^l(\Omega, \mathbb{R}^2)$ represents the $l$-compactly supported continuous-integrable function space. When $\alpha = 1$, the definition of $\mathrm{TV}^{\alpha}$ is identical to that of TV, which implies that $\mathrm{TV}^{\alpha}$ is a generalization of TV. Similarly, the $\alpha$-BV norm is defined by

$$\|u\|_{BV^{\alpha}} = \|u\|_{L^1} + TV^{\alpha}(u)$$

in [40]. Furthermore, the space of functions of $\alpha$-bounded variation on $\Omega$ can be defined by

$$BV^{\alpha}(\Omega) := \left\{ u \in L^1(\Omega) | TV^{\alpha}(u) < +\infty \right\}.$$

In [40], for any positive integer $p \in \mathbb{N}^+$, $Q_p^{\alpha}(\Omega) = \left\{ u \in L^p(\Omega) | \|u\|_{Q_p^{\alpha}(\Omega)} < +\infty \right\}$ is defined as a function space equipped with the norm

$$\|u\|_{Q_p^{\alpha}(\Omega)} = \left( \int_{\Omega} |u|^p \mathrm{d}x_1 \mathrm{d}x_2 + \int_{\Omega} |\nabla^{\alpha} u|^p \mathrm{d}x_1 \mathrm{d}x_2 \right)^{1/p},$$

where $\nabla^{\alpha} u = \left( \frac{\partial^{\alpha} u}{\partial x_1^{\alpha}}, \frac{\partial^{\alpha} u}{\partial x_2^{\alpha}} \right)^T$.

**Proposition 1** *Assume that $u \in Q_1^{\alpha}(\Omega)$; then $TV^{\alpha}(u) = \int_{\Omega} |\nabla^{\alpha} u| \mathrm{d}x$.*

**Proposition 2** *The functional $TV^{\alpha}(u)$ is convex.*

**Theorem 1** (Weak* convergence in $BV^{\alpha}(\Omega)$) *Let $\{u_k\}_{k \in \mathbb{N}}$ and $u$ belong to $BV^{\alpha}(\Omega)$. The sequence $\{u_k\}_{k \in \mathbb{N}}$ converges to $u$ weakly* in $BV^{\alpha}(\Omega)$ if $u_k \to u$ in $L^1(\Omega)$ and $\int_{\Omega} \mathbf{v} \cdot \nabla^{\alpha} u_k \mathrm{d}x \to \int_{\Omega} \mathbf{v} \cdot \nabla^{\alpha} u \mathrm{d}x$ weakly* holds for all $\mathbf{v} \in \left( C_0^0(\Omega, \mathbb{R}^2) \right)^2$, as $k \to \infty$.*

The following theorem states the compactness result corresponding to weak* convergence in $BV^{\alpha}(\Omega)$.

**Theorem 2** (Compactness in $BV^{\alpha}(\Omega)$) *Suppose that the sequence $\{u_k\}_{k \in \mathbb{N}}$ is bounded in $BV^{\alpha}(\Omega)$. Then there exist a subsequence $\{u_{k_l}\}_{l \in \mathbb{N}}$ and a function $u \in BV^{\alpha}(\Omega)$ such that $\{u_{k_l}\}_{l \in \mathbb{N}}$ converges to $u$ weakly* in $BV^{\alpha}(\Omega)$.*

Based on these results, the authors of [40] proposed the following energy functional, which involves the semi-$BV^{\alpha}(\Omega)$ norm as a regularization term:

$$E(u) = TV^{\alpha}(u) + \frac{\lambda}{2} \int_{\Omega} |u - z|^2 \mathrm{d}x, \quad (3)$$

where $z$ is given data, $1 < \alpha < 2$ and $\lambda \geqslant 0$ is a constant parameter. They also proved that the functional in (3) is lower semi-continuous with respect to the weak* topology of $BV^{\alpha}(\Omega)$. In addition, the functional in (3) is convex for $\lambda \geqslant 0$ and strictly convex if $\lambda > 0$. The lower semi-continuity and the convexity of $E$ give rise to the following theorem for the existence and uniqueness of a minimizer.

**Theorem 3** (Existence and uniqueness of a minimizer) *Assume that* $1 < \alpha < 2$ *and* $\lambda > 0$. *The following minimization problem associated with the functional in* (3),

$$\min_{u \in BV^{\alpha}(\Omega)} E(u) \tag{4}$$

*has a solution* $u \in BV^{\alpha}(\Omega)$. *Moreover, if* $\lambda > 0$, *then the solution to the minimization problem in* (4) *is unique.*

## 3 Description of the Proposed Model and the SAV Algorithm

In this section, we propose a hybrid variational model for image SR that makes use of TV regularization and fractional order regularizer. The existence of the solution of the model comprising two convex regularizers is analyzed. We also present a stable and efficient iterative algorithm for solving the problem.

### 3.1 Mathematical Model

In our proposed framework, the fidelity term based on half-quadratic estimation and the TV-$L^2$ regularization term based on the $L^2$-norm of TV and fractional order bounded variation are combined to estimate the HR image from a LR image.

Specifically, we consider the hybrid total variation (HTV) regularizer defined as

$$F^{HTV}(u) = \frac{\epsilon}{2} \int_{\Omega} |\nabla u|^2 \mathrm{d}x + \beta TV^{\alpha}(u) \tag{5}$$

with $\epsilon > 0$, $\beta > 0$, $1 < \alpha < 2$. The first term is used to preserve smooth regions of HR images. In order to preserve some fine details like textures, we add the fractional-order regularization into the model.

Furthermore, we propose the following variational problem, which is composed of the hybrid functional $F^{HTV}$ and a convex data-fidelity term,

$$\min_{u \in BV^{\alpha}(\Omega) \cap H^1(\Omega)} F(u) := F^{HTV}(u) + \frac{\lambda}{2} \int_{\Omega} (f - Hu)^2 \mathrm{d}x, \tag{6}$$

where $f \in L^2(\Omega)$ is the given LR image, $H : L^2(\Omega) \to L^2(\Omega)$ is a bounded linear operator, and $\lambda > 0$ is a constant parameter.

Thus, our model has the advantage of better restoring (less staircase effects) in smooth regions due to TV-$L^2$ regularization and the advantage of preserving textures due to the fractional order regularization.

Equivalently, we consider the following variational problem:

$$\min_{u \in \mathbb{R}^{|\Omega|}} F(u) := \sum_{(i,j) \in \Omega} \frac{\epsilon}{2} |(\nabla u)_{i,j}|^2 + \beta |(\nabla^{\alpha} u)_{i,j}| + \frac{\lambda}{2} |(f - Hu)_{i,j}|^2, \tag{7}$$

where $\Omega$ is a two-dimensional index set representing the image domain. By $|\Omega|$ we denote its cardinality.

***Remark 1*** In fact, if the operator $H$ is a blurring operator, then $f$ is defined in $\Omega$. However, when $H$ is a down-sampling linear operator, $f$ is defined in the region $\Omega_L$, which is a subset of $\Omega$. In (7), we compute $\sum_{(i,j) \in \Omega} |(f - Hu)_{i,j}|^2$ by $s^2 \sum_{(i,j) \in \Omega_L} |(f - Hu)_{i,j}|^2$, where $s$ is the scale factor in down-sampling operator.

**Theorem 4** (Existence of solution) *Assume that* $\epsilon > 0$, $\beta > 0$, $1 < \alpha < 2$, $\lambda > 0$ *and*

$$\mathrm{Ker}\nabla \cap \mathrm{Ker}\nabla^{\alpha} \cap \mathrm{Ker}H = \{0\}. \tag{8}$$

*Then there exists a global minimizer for the variational problem* (7).

***Proof*** Since $F$ is bounded from below, it suffices to show that $F$ is coercive, i.e. $F(u^k) \to +\infty$ whenever $\|u^k\| \to +\infty$ for the sequence $\{u^k\}_{k\in\mathbb{N}}$ in $\mathbb{R}^2$. We prove this by contradiction. For this purpose, assume that $\|u^k\| \to +\infty$ and that $\{F(u^k)\}_{k\in\mathbb{N}}$ is uniformly bounded. For each $k$, let $u^k = s^k v^k$ such that $s^k \geqslant 0$, $v^k \in \mathbb{R}^2$, and $\|v^k\| = 1$. For a sufficient large $k$, we have

$$\begin{aligned} 0 \leq & \frac{\epsilon}{2s_k^2}|(\nabla u_k)_{i,j}|^2 + \frac{\beta}{s_k}|(\nabla^{\alpha} u_k)_{i,j}| + \frac{\lambda}{2s_k^2}|(Hu_k)_{i,j}|^2 \\ \leq & \left(\frac{\epsilon}{2} + \beta + \frac{\lambda}{2}\right)\left(|(\nabla u_k)_{i,j}|^2 + |(\nabla^{\alpha} u_k)_{i,j}| + |(Hu_k)_{i,j}|^2\right) \to 0. \end{aligned}$$

This fact leads to

$$\lim_{k\to+\infty} \sum_{(i,j)\in\Omega} \left(\frac{\epsilon}{2}|(\nabla v_k)_{i,j}|^2 + \beta|(\nabla^{\alpha} v_k)_{i,j}| + \frac{\lambda}{2}|(Hv_k)_{i,j}|^2\right) = 0.$$

By compactness, the sequence $\{v^k\}_{k\in\mathbb{N}}$ has an accumulation point $v^*$ with $\|v^*\| = 1$ such that $v^* \in \mathrm{Ker}\nabla \cap \mathrm{Ker}\nabla^{\alpha} \cap \mathrm{Ker}H$. This contradicts our hypothesis (8). Hence, $F$ is coercive.

Next, we denote $c = \inf_{u\in\mathbb{R}^{|\Omega|}} F(u)$. Then there exist $u_m \in \mathbb{R}^{|\Omega|}$ such that

$$c \leq F(u_m) < c + \frac{1}{m}, \quad m = 1, 2, 3, \ldots$$

From the coerciveness of $F$, there exists a positive constant $b$ such that $F(u) > c + 1$ holds for $\|u\| > b$. Hence, we have $u_m \in B_b(0) \subseteq \mathbb{R}^{|\Omega|}$. By the sequential compactness of $\bar{B}_b(0)$, there exists $u^* \in \bar{B}_b(0)$ such that $\lim_{m\to+\infty} u_m \to u^*$. Then we have $c \leq F(u^*) = \lim_{m\to+\infty} F(u_m) \leq c + \frac{1}{m} \to c$. This means that $u^*$ is a global minimizer for the variational problem (7). □

***Remark 2*** One can readily know that the model (6) is strictly convex, that can guarantee a unique minimizer.

***Remark 3*** The remainder of this section is devoted to designing and analyzing an algorithm for numerically finding the minimizer of (6). In this paper, we solve problem (6) by adopting the SAV approach proposed in [38].

### 3.2 SAV Algorithm for Solving the Approximated Problem (6)

In fact, the SAV approach is a new tool for solving the minimization problem for a free energy functional $E(u)$, which is bounded from below. Denote its variational derivative as $\mu = \delta E/\delta u$. The $L^2$ gradient flow can be written as

$$\frac{\partial u}{\partial t} = -\mu, \tag{9}$$

Usually, the free energy functional contains a quadratic term, which can be written as

$$E(u) = \frac{1}{2}(u, Lu) + E_1(u), \tag{10}$$

where $L$ is a symmetric non-negative linear operator (also independent of $u$), and $E_1[u]$ are nonlinear. In the proposed model (6), we can regard $L = -\epsilon\Delta$. In addition, the Euler-Lagrange derivative of the TV$^\alpha$-term is not well defined at points where $\nabla^\alpha u = 0$, due to the presence of the term $\frac{1}{|\nabla^\alpha u|}$. Then, it is common to slightly perturb the TV$^\alpha$ functional to become

$$\int_\Omega \sqrt{|\nabla^\alpha u|^2 + \epsilon_1}\mathrm{d}x,$$

where $\epsilon_1$ is a sufficiently small positive parameter.

In order to employ the SAV approach, the free energy $E_1(u)$ should be bounded from below, i.e, there exists a constant $C_0$ such that $E_1(u) \geqslant C_0 > 0$. Therefore, we modify $E_1$ by adding a positive constant $C_0$ to $E_1$ without altering the gradient flow.

Consequently, we take $E_1(u) = \int_\Omega F_1(u)\mathrm{d}x + C_0$, where

$$F_1(u) = \beta\sqrt{|\nabla^\alpha u|^2 + \epsilon_1} + \frac{\lambda}{2}(f - Hu)^2$$

and $C_0$ is a positive constant.

Then, we employ the SAV approach to solve the proposed variational problem. Specifically, we consider (9) with the free energy in the form of

$$E[u(x)] = \int_\Omega \left[\frac{\epsilon}{2}|\nabla u|^2 + F_1(u)\right]\mathrm{d}x + C_0,$$

and the corresponding gradient flow in $L^2$:

$$\begin{aligned} \frac{\partial u}{\partial t} &= -\mu, \\ \mu &= \delta E/\delta u = -\epsilon\Delta u + F_1'(u). \end{aligned} \tag{11}$$

First, we introduce a scalar auxiliary variable $r = \sqrt{E_1(u)}$. Then we rewrite the gradient flow (10) as

$$\frac{\partial u}{\partial t} = -\mu, \tag{12}$$

$$\mu = -\epsilon\Delta u + \frac{r}{\sqrt{E_1(u)}}F_1'(u), \tag{13}$$

$$\frac{\mathrm{d}r}{\mathrm{d}t} = \frac{1}{2\sqrt{E_1(u)}}\int_\Omega F_1'(u)u_t\mathrm{d}x. \tag{14}$$

Take the time step as $\Delta t$, we solve $(u^{n+1}, \tilde{r}^{n+1})$ by using the following first-order scheme:

$$\frac{u^{n+1} - u^n}{\Delta t} = -\mu^{n+1}, \tag{15}$$

$$\mu^{n+1} = -\epsilon\Delta u^{n+1} + \frac{\tilde{r}^{n+1}}{\sqrt{E_1(u^n)}}F_1'(u^n), \tag{16}$$

$$\frac{\tilde{r}^{n+1} - r^n}{\Delta t} = \frac{1}{2\sqrt{E_1(u^n)}}\int_\Omega F_1'(u^n)\frac{u^{n+1} - u^n}{\Delta t}\mathrm{d}x. \tag{17}$$

Inspired by the work of [41], we update $r^{n+1}$ via

$$r^{n+1} = \sqrt{E_1(u^{n+1})}. \tag{18}$$

In fact, the SAV scheme (15)–(17) is easy to implement. Indeed, taking (16) and (17) into (15), we obtain

$$\frac{u^{n+1}-u^n}{\Delta t} = \epsilon \Delta u^{n+1} - \frac{F_1'(u^n)}{\sqrt{E_1(u^n)}}\left[r^n + \int_\Omega \frac{F_1'(u^n)}{2\sqrt{E_1(u^n)}}(u^{n+1}-u^n)\mathrm{d}x\right]. \tag{19}$$

Denote

$$b^n = F_1'(u^n)/\sqrt{E_1(u^n)}.$$

Then the above equation can be written as

$$(I - \Delta t\epsilon\Delta)u^{n+1} + \frac{\Delta t}{2}b^n(b^n, u^{n+1}) = u^n - \Delta t r^n b^n + \frac{\Delta t}{2}(b^n, u^n)b^n. \tag{20}$$

Denote the righthand side of (20) by $c^n$. Multiplying (20) with $(I - \Delta t\epsilon\Delta)^{-1}$, then taking the inner product with $b^n$, we obtain

$$(b^n, u^{n+1}) + \frac{\Delta t}{2}\gamma^n(b^n, u^{n+1}) = (b^n, (I - \Delta t\epsilon\Delta)^{-1}c^n), \tag{21}$$

where $\gamma^n = -(b^n, -(I - \Delta t\epsilon\Delta)^{-1}b^n) = (b^n, (I - \epsilon\Delta t\Delta)^{-1}b^n) > 0$. Hence

$$(b^n, u^{n+1}) = \frac{(b^n, (I - \Delta t\epsilon\Delta)^{-1}c^n)}{1 + \Delta t\gamma^n/2}. \tag{22}$$

To summarize, we implement (15)–(17) as follows:

(i) Compute $b^n$ and $c^n$ [the righthand side of (20)];
(ii) Compute $(b^n, u^{n+1})$ from (22);
(iii) Compute $u^{n+1}$ from (20).

***Remark 4*** According to (i) and (iii), we only need to solve, twice, a linear equation with constant coefficients of the form

$$(I - \Delta t\epsilon\Delta)\bar{x} = \bar{b}. \tag{23}$$

Therefore, the scheme is easy to implement.

Multiplying the three equations (15)–(17) by $\mu^{n+1}$, $(u^{n+1}-u^n)/\Delta t$, $2\tilde{r}^{n+1}$, integrating the first two equations, and adding them together, we derive the following stability result.

**Theorem 5** *Scheme* (15)–(17) *is first-order accurate and unconditionally energy stable in the sense that*

$$\begin{aligned}&\frac{1}{\Delta t}[\tilde{E}(u^{n+1}, \tilde{r}^{n+1}) - \tilde{E}(u^n, r^n)]\\ &\quad + \frac{1}{\Delta t}\left[\frac{\epsilon}{2}(u^{n+1}-u^n, -\Delta(u^{n+1}-u^n)) + (\tilde{r}^{n+1}-r^n)^2\right]\\ &\quad = -(\mu^{n+1}, \mu^{n+1}),\end{aligned}$$

*where* $\tilde{E}(u, r) = -\frac{\epsilon}{2}(u, \Delta u) + r^2$ *is the modified energy, and one can obtain* $(u^{n+1}, \tilde{r}^{n+1})$ *by solving two linear equations with constant coefficients of the form* (23).

***Remark 5*** The above result does not imply that the scheme (15)–(18) is energy diminishing, since we can not prove $\tilde{E}(u^{n+1}, r^{n+1}) \leqslant \tilde{E}(u^n, r^n)$. However, if we do not perform the update in (18) and replace $\tilde{r}^{n+1}$ by $r^{n+1}$ in (17), then the scheme is energy diminishing with $\tilde{E}(u^{n+1}, r^{n+1}) \leqslant \tilde{E}(u^n, r^n)$.

### 3.3 Time-Step Adaptivity

Time-step adaptivity is of prime importance to simulate the entire dynamics of the Cahn–Hilliard equation [42,43], accurately and efficiently. Similarly, we propose an adaptive time-stepping strategy for our provably stable scheme. The method is presented in Algorithm 1. We update the time step size by using the formula

$$A_{d\rho}(e, \tau) = \rho \left( \frac{tol}{e} \right)^{1/2} \tau,$$

where $\rho$ is a default safety coefficient, $tol$ is a reference tolerance, and $e$ is the relative error at each time level. In this paper, we choose $\rho = 0.8$ and $tol = 0.07$. The minimum and maximum time steps are taken as $\tau_{min} = 10^{-4}$ and $\tau_{max} = 10^{-1}$, respectively. The initial time step is taken as $\tau_{min}$.

**Algorithm 1** SAV algorithm with adaptive time step strategy

given $\epsilon$, $\beta$, $\beta_1$, $\alpha$, $\lambda$, $tol$, $\rho$, $\tau_{min}$, $\tau_{max}$
compute $u^{n+1}$ by the first order SAV scheme with $\tau_n$
calculate $Ey^{n+1} = E(u^{n+1})$
calculate $e_{n+1} = ||Ey^n - Ey^{n+1}||/||Ey^{n+1}||$
**if** $e_{n+1} > tol$ **then**
    recalculate time step $\tau_n = \max\{\tau_{min}, \min\{A_{d\rho}(e_{n+1}, \tau_n), \tau_{max}\}\}$ go to step 2
**else**
    update $\tau_{n+1} = \max\{\tau_{min}, \min\{A_{d\rho}(e_{n+1}, \tau_n), \tau_{max}\}\}$ Stop; or set $n = n + 1$ and go to step 2
**end if**
**return**

### 3.4 Space discretization of the scheme

In this subsection, we introduce the space discretization of SAV scheme (15)–(17) at each iteration. For practical applications, we first assume that the initial discrete image $u$ is $m \times m$ pixels, and that it has been sampled from its continuous version at uniformly spaced points starting at $(0, 0)$, i.e., $u(x_1, x_2) = u(x_1 \Delta x_1, x_2 \Delta x_2)$ for $x_1, x_2 = 0, 1, \ldots, m - 1$. The grid size $\Delta x_1$ and $\Delta x_2$ is chosen as $\Delta x_1 = \Delta x_2 = 1$. According to the scheme (15)–(17), we present the computation for $\Delta u^{n+1}$, $E_1(u^n)$ and $F_1'(u^n)$. After considering the input image as a periodic image, we apply fast Fourier transform to compute $\Delta u^{n+1}$ for a given $u^{n+1}$.

In order to compute $E_1(u^n)$ and $F'(u^n)$, we need introduce the computation for the fractional-order difference $\nabla^\alpha u$ for a given image $u$. For convenience, we use the notation $\mathcal{F}$ to denote the 2-D discrete Fourier transform operator and the notation $\mathcal{F}^{-1}$ to denote the 2-D inverse discrete Fourier transform operator. Then we use the central difference scheme in [36] to compute the fractional-order difference, which can be defined as

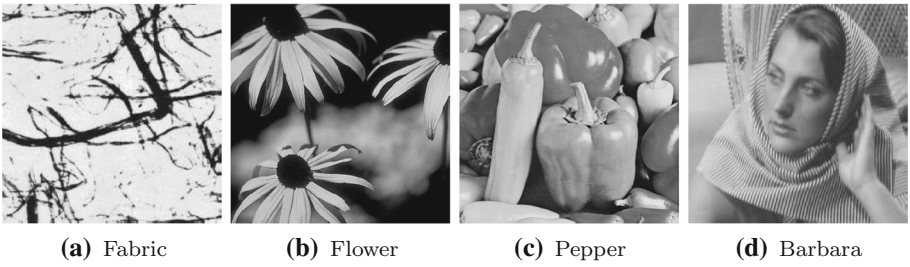

**(a)** Fabric **(b)** Flower **(c)** Pepper **(d)** Barbara

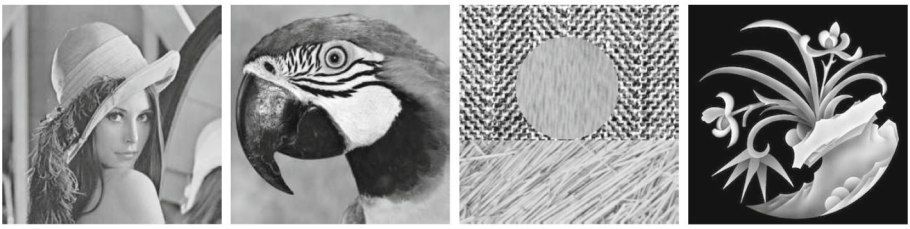

**(e)** Lena **(f)** Parrot **(g)** Synthetic **(h)** Timg

**Fig. 1** Original images

$$\begin{aligned} D_x^\alpha u &= \mathcal{F}^{-1}((1-\exp(-i2\pi\omega_1/m))^\alpha \times \exp(i\pi\alpha\omega_1/m)\mathcal{F}(u)), \\ D_y^\alpha u &= \mathcal{F}^{-1}((1-\exp(-i2\pi\omega_2/m))^\alpha \times \exp(i\pi\alpha\omega_2/m)\mathcal{F}(u)). \end{aligned} \tag{24}$$

To simplify, let $K_1$ be a purely diagonal operator in the frequency domain defined by

$$K_1 = \mathrm{diag}((1-\exp(-i2\pi\omega_1/m))^\alpha \times \exp(i\pi\alpha\omega_1/m)),$$

where diag($\mathbf{v}$) means creating a diagonal matrix with the elements of vector $\mathbf{v}$. Then we get the following equivalent expression

$$D_x^\alpha = \mathcal{F}^{-1} \circ K_1 \circ \mathcal{F}. \tag{25}$$

Denote $D_x^{\alpha *}$ as the adjoint of $D_x^\alpha$, then we obtain

$$D_x^{\alpha *} = \mathcal{F}^{-1} \circ K_1^* \circ \mathcal{F}.$$

Since $K_1$ is a purely diagonal operator and $K_1^*$ is the complex conjugation of $K_1$, we have

$$\begin{aligned} D_x^{\alpha *} u &\leftrightarrow \mathrm{conj}((1-\exp(-i2\pi\omega_1/m))^\alpha \times \exp(i\pi\alpha\omega_1/m))\mathcal{F}u(\omega_1,\omega_2), \\ D_y^{\alpha *} u &\leftrightarrow \mathrm{conj}((1-\exp(-i2\pi\omega_2/m))^\alpha \times \exp(i\pi\alpha\omega_2/m))\mathcal{F}u(\omega_1,\omega_2), \end{aligned}$$

where conj$(\cdot)$ is the complex conjugation.

Then, according to (7) and remark 1, we can compute $E_1(u^n)$ by

$$E_1(u^n) = \sum_{(i,j)\in\Omega} -\frac{\epsilon}{2}(u^n)_{i,j}(\Delta u^n)_{i,j} + \beta|(\nabla^\alpha u^n)_{i,j}| + \frac{\lambda s^2}{2}\sum_{(i,j)\in\Omega_L}|(f-Hu^n)_{i,j}|^2,$$

where $\nabla^\alpha u^n = (D_x^\alpha u^n, D_y^\alpha u^n), |(\nabla^\alpha u^n)_{i,j}| = \sqrt{(D_x^\alpha u^n)_{i,j}^2 + (D_y^\alpha u^n)_{i,j}^2}$, $s$ is the scale factor in down-sampling operator.

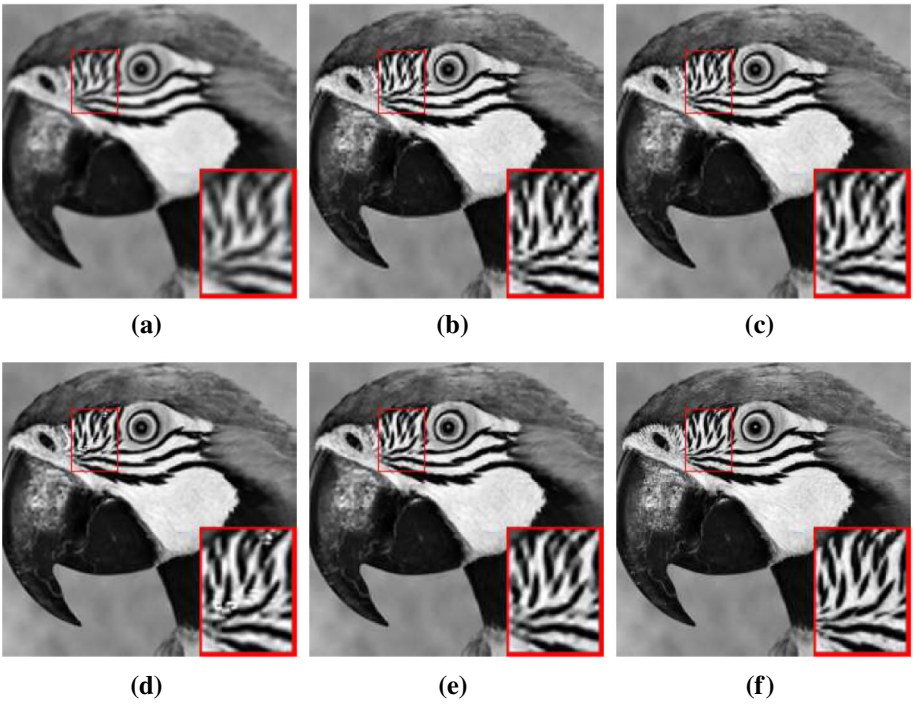


**Fig. 2** SR results (Gaussian kernel, $\times 2$) of Parrot by different methods. **a** LR image **b** WBM [44] (26.8 dB) **c** TVRBM [44] (27.2 dB) **d** SRBM [45] (27.8 dB) **e** ours (28.2 dB, 319 iterations) **f** original image

Furthermore, we compute $F_1'(u^n)$ by

$$F_1'(u^n) = \beta D_x^{\alpha *}\left(\frac{D_x^{\alpha} u^n}{\sqrt{|\nabla^{\alpha} u^n|^2 + \epsilon_1}}\right) + \beta D_y^{\alpha *}\left(\frac{D_y^{\alpha} u^n}{\sqrt{|\nabla^{\alpha} u^n|^2 + \epsilon_1}}\right) + \lambda H'(Hu^n - f),$$

where $H'$ is the transpose operator to $H$.

## 4 Numerical Experiments

In this section, we present numerical results for the model we proposed in (7), tested on several images.

### 4.1 Experimental Settings

In the experiments of super-resolution, the degraded LR images were generated by first applying a truncated $15 \times 15$ Gaussian kernel of standard deviation 1 to the original image and then down-sampling by a factor of 2. We compare the proposed method with three state-of-the-art methods: wavelet based method (WBM) [44], TV regularization based method (TVRBM) [44] and sparse representation based method (SRBM) [45]. In the proposed variational based super-resolution, the parameters are set as follows. For the noiseless LR images, we empirically set $\alpha = 1.1$, $\beta = 1$, $\lambda = 40$, $\epsilon = 10^{-18}$, $\epsilon_1 = 10^{-9}$. Empirically, we take the stopping criterion as $t_n > T_{tol} = 20$, where $t_n = \sum_{i=1}^{n} \tau_i$.

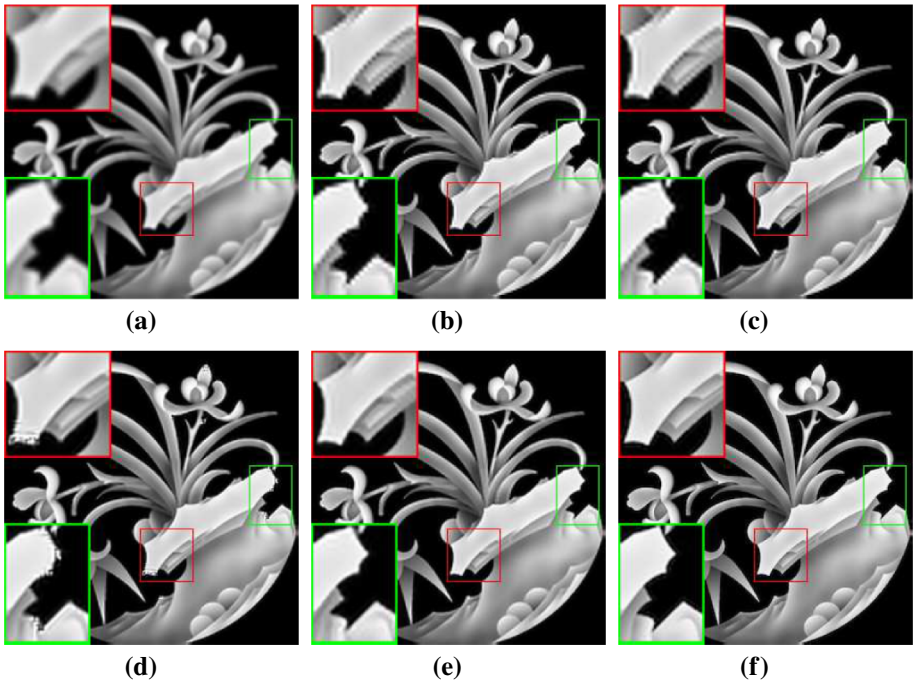


**Fig. 3** SR results (Gaussian kernel, $\times 2$) of Timg by different methods. **a** LR image **b** WBM [44] (26.7 dB) **c** TVRBM [44] (27.2 dB) **d** SRBM [45] (29.4 dB) **e** ours (30.2 dB, 318 iterations) **f** original image

PSNR (Peak Signal to Noise Ratio, unit: dB) [46] is used to evaluate the objective image quality.We recommend the reader to carefully examine the different parts of the images (constant areas, sharp edges, small details and oriented textures) to observe how these parts are restored (Fig 1).

### 4.2 Experimental Results on Single-Image Super-Resolution

Reconstructed HR images by the TV-regularization-based method in [44] have many jaggy and ringing artifacts. Therefore, they fail to reconstruct fine image edges. It is observed that the reconstructed edges by [44] are relatively smooth and some fine image structures are not recovered. The sparse representation based method [45] is effective in suppressing the ringing artifacts, but it damages some edges of images, see Figs. 2, 3 and 4. The proposed method leads to the best visual quality. It can not only remove the blurring effects, but also reconstruct more and sharper image edges than other methods. The excellent edge and detail preservation owes to the fractional order $TV^{\alpha}$ regularizations.

In Table 1, we present the comparison of the corresponding PSNR values and CPU times for results in Figs. 2, 3 and 4. All simulations listed here are run in MATLAB 8.5 (R2015a) on a PC equipped with 2.90 GHz CPU and 8 G RAM memory. As presented in Table 1, the proposed model delivers the best results in a relatively short amount of time due to few iterations (about 319 iterations).

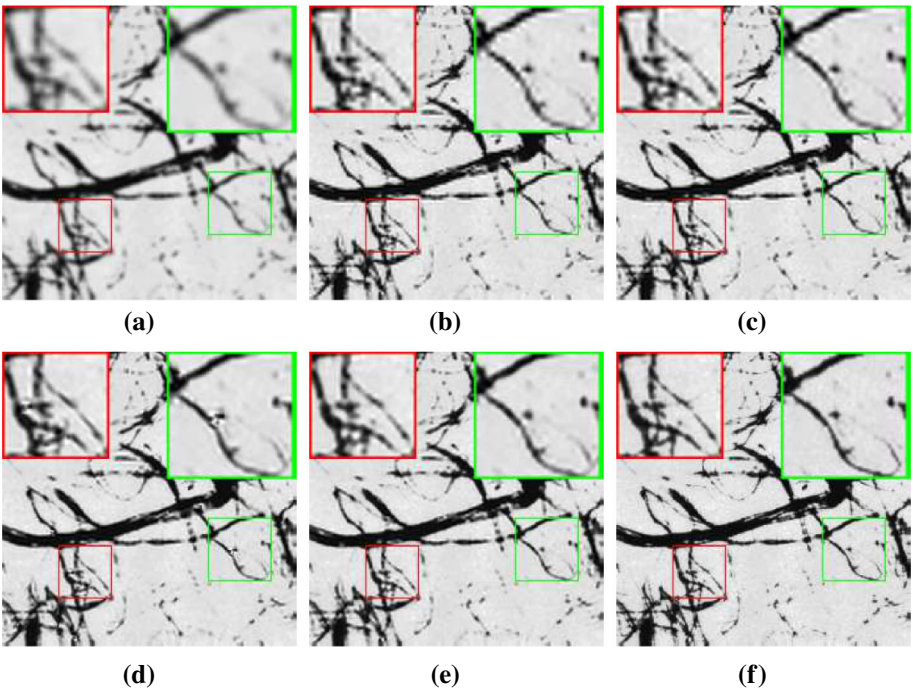


**Fig. 4** SR results (Gaussian kernel, $\times 2$) of Fabric by different methods. **a** LR image **b** WBM [44] (24.1 dB) **c** TVRBM [44] (24.5 dB) **d** SRBM [45] (25.2 dB) **e** ours (26.2 dB, 319 iterations) **f** original image

**Table 1** Comparison of PSNR and CPU time

| Index | PSNR(dB) | | | CPU time(s) | | |
|---|---|---|---|---|---|---|
| Test images | Parrot | Timg | Fabric | Parrot | Timg | Fabric |
| WTBM [44] | 26.8 | 26.7 | 24.1 | 1.39 | 6.03 | 2.44 |
| TVRBM [44] | 27.2 | 27.2 | 24.5 | 0.33 | 0.57 | 0.41 |
| SRBM [45] | 27.8 | 29.4 | 25.2 | 360.4 | 513.45 | 408.42 |
| Ours | 28.2 | 30.2 | 26.2 | 44.43 | 62.14 | 44.84 |

**Table 2** Comparison of the PSNR (dB) of the recovered results by different methods, with respect to the scaling parameter $s = 2$

| Image | WTBM [44] | TVRBM [44] | SRBM [45] | Ours |
|---|---|---|---|---|
| Fab. | 24.1 | 24.5 | 25.2 | 26.2 |
| Flo. | 30.6 | 30.9 | 32.3 | 32.1 |
| Pep. | 34.0 | 34.3 | 35.5 | 35.3 |
| Bar. | 23.6 | 23.3 | 23.3 | 23.5 |
| Lena | 30.3 | 30.7 | 32.4 | 31.6 |
| Parr. | 26.8 | 27.2 | 27.8 | 28.2 |
| Syn. | 21.9 | 22.4 | 22.4 | 23.0 |
| Timg | 26.7 | 27.2 | 29.4 | 30.2 |
| Aver. | 27.25 | 27.56 | 28.54 | 28.75 |

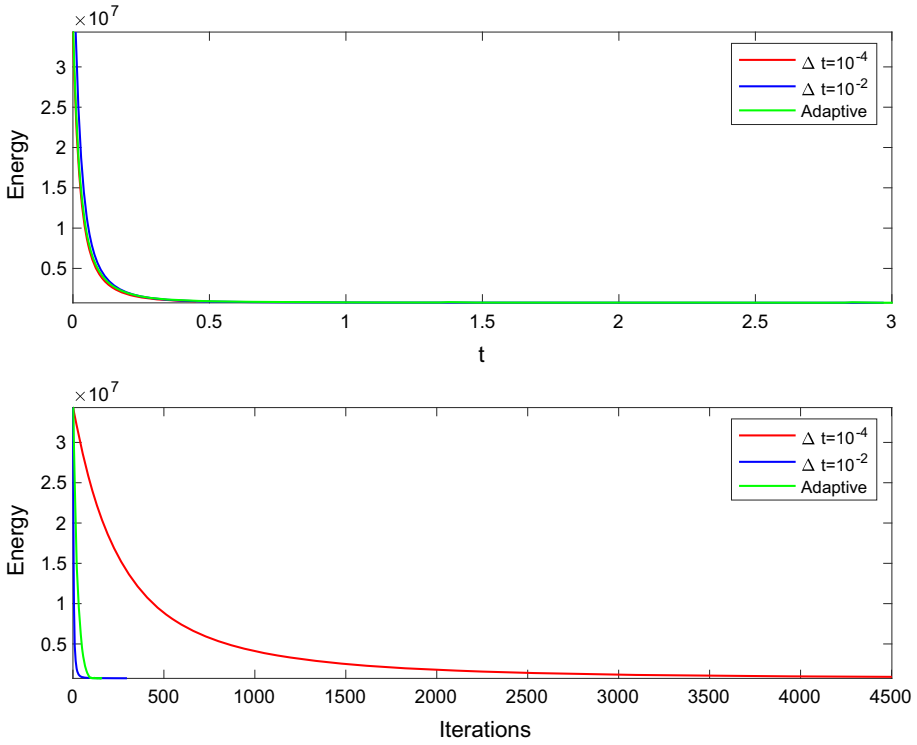


**Fig. 5** Parrot SR: comparisons among small time steps, adaptive time steps, and large time steps

The PSNR results by different methods are listed in Table 2. For the experiments using Gaussian kernel, the average PSNR improvements of the proposed method over other three methods are 0.21 dB at least.

### 4.3 Efficiency of the Adaptive Time Stepping Strategy

In order to illustrate the efficiency of the adaptive time stepping strategy, we apply the SAV algorithm to reconstruct three test images (Fabric, Parrot and Timg) from degraded LR images generated as we mentioned before. In the experiment, we take $\tau_{\min} = 10^{-4}$, $\tau_{\max} = 10^{-1}$, $tol = 0.07$, $\rho = 0.8$ for adaptive time stepping strategy. For comparison, we also apply the SAV algorithm with a small uniform time step $\Delta t = 10^{-4}$ and a large uniform time step $\Delta t = 10^{-2}$.

We present the energy evolutions by using different kinds of time stepping in Figs. 5, 6 and 7. As shown these figures, the energy of numerical solutions decrease with time increasing and finally converge to the same final steady state. In addition, we observe that the algorithm with adaptive time stepping needs the least iterations to converge to steady state. In addition, we present comparison of the total number of iterations and corresponding CPU time in Table 3. Table 3 illustrates that the algorithm with adaptive time steps consumes least CPU time and the total number of iterations among three computing methods. This means that the SAV scheme with adaptive time stepping is more efficient than other two computing methods. Furthermore, Fig. 8 implies that the time step changes accord-

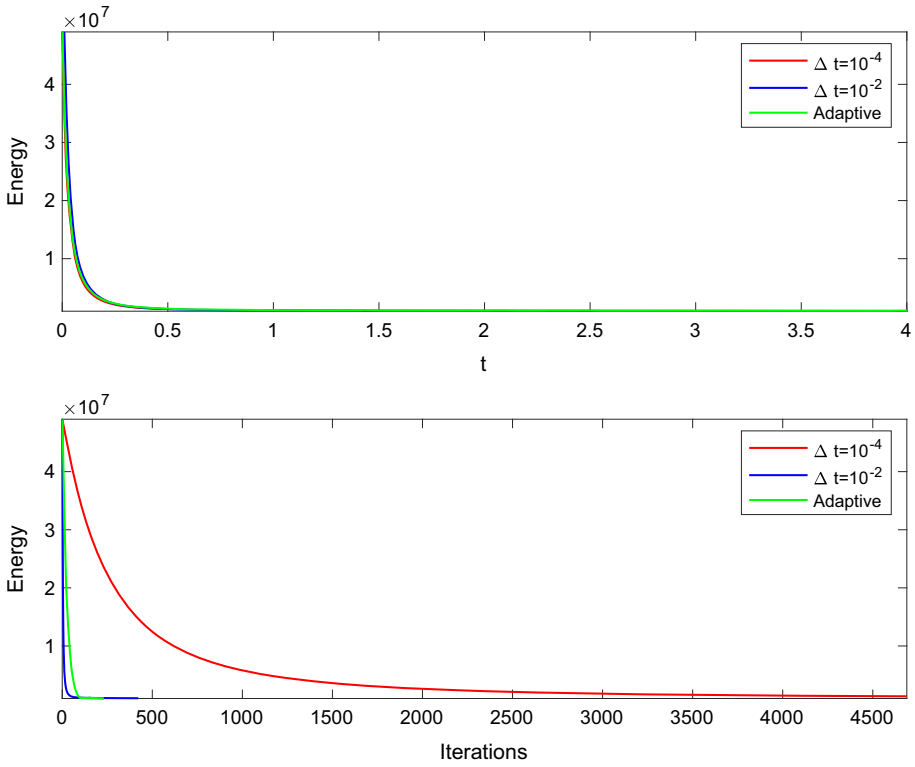


**Fig. 6** Timg SR: comparisons among small time steps, adaptive time steps, and large time steps

ingly with the energy evolution. There are almost three-orders of magnitude variation in the time step, which indicates that the adaptive time stepping for the SAV schemes is very efficient.

## 5 Conclusion

We proposed a hybrid TV and total $\alpha$-order variation based minimization models for single image super resolution. Our model consists of a convex data-fidelity term and the TV-$L^2$ norm regularization term and total $\alpha$-order variation regularization term. The proposed model eliminates the staircasing artifacts commonly appeared in the results of TV-based models. Moreover, the proposed hybrid model can produce better preserved edges, textures, and fine features in the restored images. We proved the existence and uniqueness of the minimizers for the proposed model.

We developed efficient iterative algorithms using the SAV approach with adaptive time steps to handle the complicated data fidelity term and total $\alpha$-order variation regularization term. Although we only considered semi-discretization in time in this paper, all the results can be extended to fully discretized schemes as long as the spatial discretization respect integration by parts, since our proofs are variational with simple test functions.

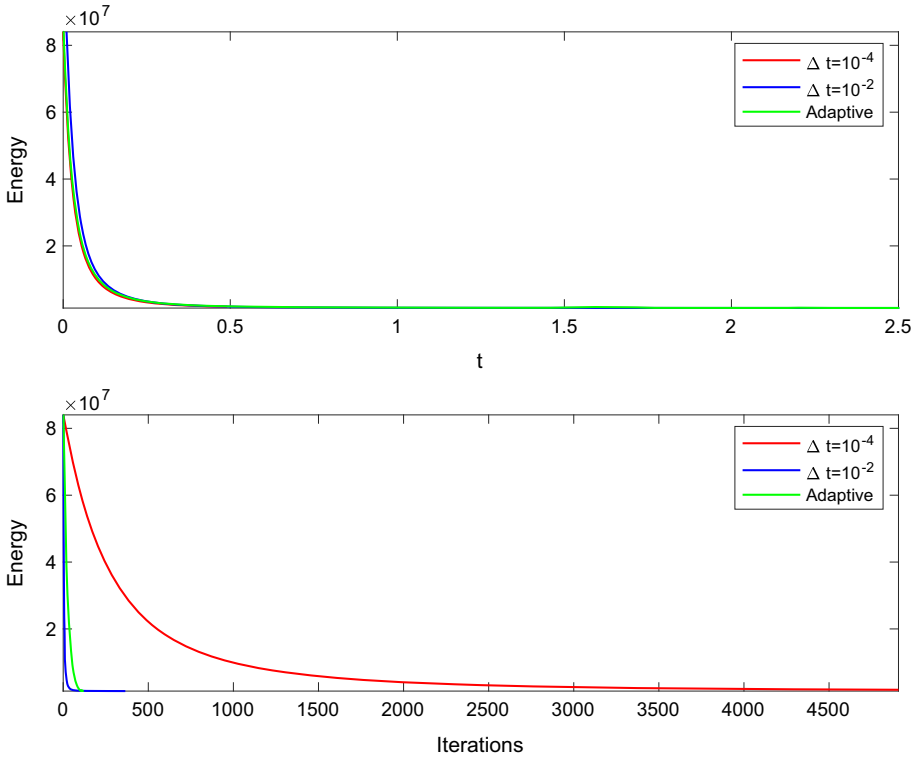


**Fig. 7** Timg SR: comparisons among small time steps, adaptive time steps, and large time steps

**Table 3** Comparison of the total number of iterations and CPU time in Figs. 5, 6, and 7

| Index | Total number of iterations | | | CPU time(s) | | |
|---|---|---|---|---|---|---|
| Test images | Parrot | Timg | Fabric | Parrot | Timg | Fabric |
| $\Delta t = 10^{-4}$ | 4502 | 4689 | 4908 | 433.27 | 624.98 | 466.53 |
| $\Delta t = 10^{-2}$ | 297 | 461 | 251 | 27.77 | 51.29 | 22.76 |
| Adaptive step | 120 | 131 | 119 | 14.80 | 23.99 | 14.92 |

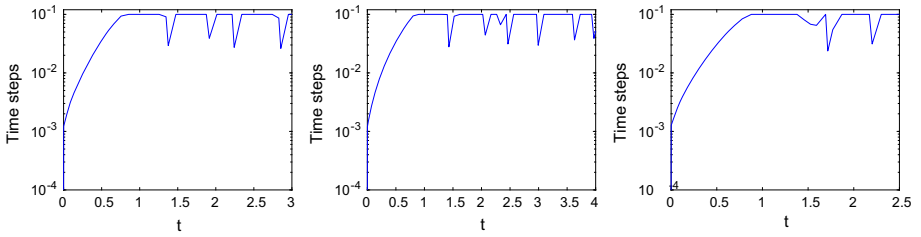


**(a)** Result of Parrot SR **(b)** Result of Timg SR **(c)** Result of Fabric SR

**Fig. 8** Adaptive time steps

The proposed model and numerical scheme are able to effectively smoothing homogeneous regions while preserving edges and textures, and they provide better HR results for both natural images and synthetic images when compared with other approaches.

**Acknowledgements** This work is partially supported by the National Natural Science Foundation of China (11971131, 11971407, U1637208, 61873071, 51476047, 11871133), NSF DMS-1720442, the Natural Science Foundation of Heilongjiang Province (LC2018001, A2016003).

## References

1. Martín, G., Bioucas-Dias, J.M.: Hyperspectral compressive acquisition in the spatial domain via blind factorization. In: 2015 7th Workshop on Hyperspectral Image and Signal Processing: Evolution in Remote Sensing (WHISPERS). pp. 1–4 (2015)
2. Akgun, T., Altunbasak, Y., Mersereau, R.M.: Super-resolution reconstruction of hyperspectral images. IEEE Trans. Image Process. **14**(11), 1860–1875 (2005)
3. Morin, R., Basarab, A., Kouamé, D.: Alternating direction method of multipliers framework for super-resolution in ultrasound imaging. In: 2012 9th IEEE International Symposium on Biomedical Imaging (ISBI). pp. 1595–1598 (2012)
4. Park, S.C., Park, M.K., Kang, M.G.: Super-resolution image reconstruction: a technical overview. IEEE Signal Process. Mag. **20**(3), 21–36 (2003)
5. Lertrattanapanich, S., Bose, N.K.: High resolution image formation from low resolution frames using delaunay triangulation. IEEE Trans. Image Process. **11**(12), 1427–1441 (2002)
6. Hou, S., Andrews, H,C.: Cubic splines for imageinterpolation and digitalfiltering. IEEE Trans. Acoust. Speech Signal Process. **26**, 508–517 (1979)
7. Freeman, W.T., Jones, T.R., Pasztor, E.C.: Example-based super-resolution. IEEE Comput. Graphics Appl. **22**(2), 56–65 (2002)
8. Elad, M., Datsenko, D.: Example-based regularization deployed to super-resolution reconstruction of a single image. Comput. J. **52**(1), 15–30 (2018)
9. Glasner, D., Bagon, S., Irani, M.: Super-resolution from a single image. In: IEEE International Conference on Computer Vision, pp. 349–356 (2009)
10. Patanavijit, V., Jitapunkul, S.: A robust iterative multiframe super-resolution reconstruction using a bayesian approach with lorentzian norm. In: 2006 10th IEEE Singapore International Conference on Communication Systems. pp. 1–5 (2006)
11. Yue, L., Shen, H., Yuan, Q., Zhang, L.: A locally adaptive l1–l2 norm for multi-frame super-resolution of images with mixed noise and outliers. Sig. Process. **105**, 156–174 (2014)
12. Zeng, X., Yang, L.: A robust multiframe super-resolution algorithm based on half-quadratic estimation with modified btv regularization. Digit. Signal Proc. **23**(1), 98–109 (2013)
13. Wang, H., Gao, X., Zhang, K., Li, J.: Single-image super-resolution using active-sampling gaussian process regression. IEEE Trans. Image Process. **25**(2), 935–948 (2016)
14. Zhu, Z., Guo, F., Yu, H., Chen, C.: Fast single image super-resolution via self-example learning and sparse representation. IEEE Trans. Multimedia **16**(8), 2178–2190 (2014)
15. Maeland, E.: On the comparison of interpolation methods. IEEE Trans. Med. Imaging **7**(3), 213–217 (1988)
16. Lu, X., Yuan, Y., Yan, P.: Image super-resolution via double sparsity regularized manifold learning. IEEE Trans. Circuits Syst. Video Technol. **23**(12), 2022–2033 (2013)
17. Dong, C., Loy, C.C., He, K., Tang, X.: Learning a deep convolutional network for image super-resolution. In: Computer Vision–ECCV 2014, Lecture notes in computer science, vol. 8692, pp. 184–199. Springer (2014)
18. Zhang, K., Zuo, W., Chen, Y., Meng, D., Zhang, L.: Beyond a gaussian denoiser: residual learning of deep cnn for image denoising. IEEE Trans. Image Process. **26**(7), 3142–3155 (2017)
19. Zhang, K., Zuo, W., Zhang, L.: Learning a single convolutional super-resolution network for multiple degradations. In: Proceedings/CVPR, IEEE Computer Society Conference on Computer Vision and Pattern Recognition. IEEE Computer Society Conference on Computer Vision and Pattern Recognition (2018)
20. Kim, J., Lee, J.K., Lee, K.M.: Accurate image super-resolution using very deep convolutional networks. In: 2016 IEEE Conference on Computer Vision and Pattern Recognition (CVPR). pp. 1646–1654 (2016)

21. Kim, J., Lee, J.K., Lee, K.M.: Deeply-recursive convolutional network for image super-resolution. In: 2016 IEEE Conference on Computer Vision and Pattern Recognition (CVPR). pp. 1637–1645 (2016)
22. Sun, J., Xu, Z., Shum, H.-Y.: Image super-resolution using gradient profile prior. In: 2008 IEEE Conference on Computer Vision and Pattern Recognition. pp. 1–8 (2008)
23. Li, X., He, H., Wang, R., Tao, D.: Single image superresolution via directional group sparsity and directional features. IEEE Trans. Image Process. **24**(9), 2874–2888 (2015)
24. Yue, L., Shen, H., Li, J., Yuan, Q., Zhang, H., Zhang, L.: Image super-resolution: the techniques, applications, and future. Sig. Process. **128**, 389–408 (2016)
25. Zhang, X., Lam, E., Wu, E., Wong, K.: Application of tikhonov regularization to super-resolution reconstruction of brain mri images. pp. 51–56 (2007)
26. Rudin, L.I., Osher, S., Fatemi, E.: Nonlinear total variation based noiseremoval algorithms. Phys. D Nonlinear Phenom. **60**, 259–268 (1992)
27. Donoho, D.L.: Compressed sensing. IEEE Trans. Inf. Theory **52**(4), 1289–1306 (2006)
28. Hale, E.T., Yin, W., Zhang, Y.: Fixed-point continuation for $l_1$-minimization: methodology and convergence. SIAM J. Optim. **19**(3), 1107–1130 (2008)
29. Rodríguez, P., Wohlberg, B.: Efficient minimization method for a generalized total variation functional. IEEE Trans. Image Process. **18**(2), 322–332 (2009)
30. Marquina, A., Osher, S.: Image super-resolution by TV-regularization and bregman iteration. J. Sci. Comput. **37**, 367–382 (2008)
31. Chan, T., Marquina, A., Mulet, P.: High-order total variation-based image restoration. SIAM J. Sci. Comput. **22**(2), 503–516 (2000)
32. Lysaker, M., Lundervold, A., Tai, X.-C.: Noise removal using fourth-order partial differential equation with applications to medical magnetic resonance images in space and time. IEEE Trans. Image Process. **12**(12), 1579–1590 (2003)
33. Jung, M., Bresson, X., Chan, T.F., Vese, L.A.: Nonlocal mumford-shah regularizers for color image restoration. IEEE Trans. Image Process. **20**(6), 1583–1598 (2011)
34. Chan, R.H., Lanza, A., Morigi, S., Sgallari, F.: An adaptive strategy for the restoration of textured images using fractional order regularization. Nume. Math. Theory Methods Appl. **6**(1), 276–296 (2013)
35. Ren, Z., He, C., Zhang, Q.: Fractional order total variation regularization for image super-resolution. Sig. Process. **93**(9), 2408–2421 (2013)
36. Bai, J., Feng, X.C.: Fractional-order anisotropic diffusion for image denoising. IEEE Trans. Image Process. **16**(10), 2492–2502 (2007)
37. Pu, Y.F., Zhou, J.L., Yuan, X.: Fractional differential mask: a fractional differential-based approach for multiscale texture enhancement. IEEE Trans. Image Process. **19**(2), 491–511 (2010)
38. Shen, J., Xu, J., Yang, J.: The scalar auxiliary variable (SAV) approach for gradient flows. J. Comput. Phys. **353**, 407–416 (2018)
39. Shen, J., Xu, J., Yang, J.: A new class of efficient and robust energy stable schemes for gradient flows. SIAM Rev. **61**(3), 474–506 (2019)
40. Zhang, J., Chen, K.: A total fractional-order variation model for image restoration with nonhomogeneous boundary conditions and its numerical solution. SIAM J. Imaging Sci. **8**(4), 2487–2518 (2015)
41. Zhuang, Q., Shen, J.: Efficient sav approach for imaginary time gradient flows with applications to one- and multi-component bose-einstein condensates. J. Comput. Phys. **396**, 72–88 (2019)
42. Gómez, H., Calo, V.M., Bazilevs, Y., Hughes, T.J.R.: Isogeometric analysis of the Cahn–Hilliard phase-field model. Comput. Methods Appl. Mech. Eng. **197**(49–50), 4333–4352 (2008)
43. Rajagopal, A., Fischer, P., Kuhl, E., Steinmann, P.: Natural element analysis of the Cahn–Hilliard phase-field model. Comput. Mech. **46**(3), 471–493 (2010)
44. Zhao, N., Wei, Q., Basarab, A., Dobigeon, N., Kouamé, D., Tourneret, J.: Fast single image super-resolution using a new analytical solution for $\ell_2$-$\ell_2$ problems. IEEE Trans. Image Process. **25**(8), 3683–3697 (2016)
45. Dong, W., Zhang, L., Shi, G., Wu, X.: Image deblurring and super-resolution by adaptive sparse domain selection and adaptive regularization. IEEE Trans. Image Process. **20**(7), 1838–1857 (2011)
46. Durand, S., Fadili, J., Nikolova, M.: Multiplicative noise removal using l1 fidelity on frame coefficients. J. Mathemat. Imaging Vis. **36**(3), 201–226 (2010). https://doi.org/10.1007/s10851-009-0180-z